Applied Catalysis B: Environmental 158–159 (2014) 60–69

Contents lists available at ScienceDirect

Applied Catalysis B: Environmental

journal homepage: www.elsevier.com/locate/apcatb

# Ultra-high-performance doped carbon catalyst derived from *o*-phenylenediamine and the probable roles of Fe and melamine

Hongliang Peng, Sanying Hou, Dai Dang, Bingqing Zhang, Fangfang Liu, Ruiping Zheng, Fan Luo, Huiyu Song, Peiyan Huang, Shijun Liao *

*Key Lab for Fuel Cell Technology of Guangdong Province & Key Lab of New Energy Technology of Guangdong Universities, School of Chemistry and Chemical Engineering, South China University of Technology, Guangzhou 510641, China*

ARTICLE INFO

*Article history:*
Received 5 December 2013
Received in revised form 11 March 2014
Accepted 18 March 2014
Available online 4 April 2014

*Keywords:*
Doped carbon catalyst
Fuel cell
Graphene-like
Melamine
Oxygen reduction reaction

ABSTRACT

By pyrolyzing hybrid precursor of poly *o*-phenylenediamine (oPD), melamine and iron in an Ar atmosphere, a doped carbon catalyst, Fe/oPD–Mela, with high surface area, high pyridinic and graphitic nitrogen content, is prepared successfully. This catalyst exhibit high performance towards the oxygen reduction in both alkaline and acid mediums; actually its activity surpassed that of commercial Pt/C catalyst in an alkaline medium. In 0.1 M KOH, the half-wave potential is high up to 0.91 V, which is about 50 mV higher than that of Pt/C, and the current density at 0.90 V is about 2.4 times to that of the Pt/C catalyst. And in an acid medium, its activity approaches that of a Pt/C catalyst. Furthermore, this catalyst also showed high stability and impressive immunity towards methanol. The probable roles of added iron and melamine are investigated intensively; both of them are playing an important role in the ORR activity of Fe/oPD–Mela.



## 1. Introduction

Low-temperature fuel cells (LTFCs) can convert chemical energy into electrical energy without combustion and it is recognized as one of the most competitive alternative energy technologies for practical applications on a large scale, due to their high energy conversion efficiency, environmental benignity, and rapid start-up, as well as other features. Pt-based catalysts are the most popular for use in LTFCs [1–8], but the high cost and limited availability of platinum are serious hindrances at a practical level. Thus, the development of effective non-precious metal catalysts, especially doped carbon catalysts, has become one of the hottest topics in fuel cell research, attracting major attention worldwide [9–23].

Actually, some breakthroughs have been achieved for doped carbon catalysts with respect to high activity and high stability in recent years [24–33]. For example: In doped carbon nanotubes (CNT) research, Deng et al. [28] developed some Fe/Co- and N-doped CNT catalyst; the membrane electrode assembly (MEA) prepared with these catalysts at the cathode achieved stable operation for 200 h in a $H_2$-$O_2$ single polymer-electrolyte-membrane (PEM) fuel cell. Chung et al. [31] reported a Fe- and N-doped CNT catalyst synthesized by pyrolyzing a hybrid precursor of cyanamide, iron acetate, and carbon powder, the catalyst exhibited higher oxygen reduction reaction (ORR) activity and stability than that of the Pt/C catalyst in an alkaline medium. These researchers wrapped transition metals in the interior of nitrogen-doped CNT and it was considered as the key reason for the high ORR activity and stability of the catalysts. Cheon et al. [34] reported an ordered mesoporous porphyrinic carbon catalyst, which was synthesized through using ordered mesoporous silica as templates. The catalyst showed high ORR activity and stability, which were comparable with the commercial platinum catalyst in both acidic and alkaline medium. Pachfule et al. [11] reported a porous nitrogen-doped carbon catalyst by using a porous organic framework as a template, also, this catalyst exhibited high ORR activity and stability, and the ordered porous structure was recognized as a key factor for its high performance [5]. Zhang et al. [35,36] reported a CNTs and graphene composite catalyst, which was prepared by in-situ growth of CNTs in the presence of graphene sheets with Fe and melamine as precursors and this composite catalyst demonstrated the superior ORR activity to the single CNTs or graphene doped catalyst. Actually, there have been already a lot of literatures for the doped carbon, including doped graphene [37–43] catalysts recently, and these catalysts also showed good ORR activity. However, although the breakthroughs and achievements are really inspiring, there is still a long way to the practical application of doped carbon catalyst,

* Corresponding author at: South China University of Technology, College of Chemistry, Wushan, Guangzhou, Guangdong 510641, China. Tel.: +86 20 87113586; fax: +86 20 87112906/+86 20 87113586.
*E-mail address:* chsjliao@scut.edu.cn (S. Liao).

http://dx.doi.org/10.1016/j.apcatb.2014.03.033
0926-3373/

and a lot issues about the mechanism and the role of components in the catalysts are still unclear.

Previously, we reported a high-performance doped carbon catalyst, Fe-PANI/C–Mela, which was prepared by pyrolyzing of a hybrid precursor of polyaniline (PANI), melamine, and Fe [27]. Inspired by the researches mentioned above and as a continuation of our research interests in Fe and N doped graphene structure carbon catalyst [27,44] for ORR, in this paper, by attempting to use poly *o*-phenylenediamine (*o*PD) instead of polyamine, we prepared a new Fe/*o*PD–Mela catalyst by pyrolyzing the hybrid precursors of poly *o*-phenylenediamine, melamine and Fe. The poly(*o*-phenylenediamine) has a double —$NH_2$ group to polyaniline, it should be able to increase the nitrogen content of the catalyst, and may make Fe/oPM–Mela exhibited better ORR activity than our previous catalyst. Interestingly, it was confirmed by experimental results. This doped carbon catalyst Fe/*o*PD–Mela exhibited much better ORR performance in alkaline than the Fe-PANI/C–Mela catalyst we had previously reported. Indeed, its performance surpassed that of a state-of-the-art Pt/C catalyst (JM 4100) in alkaline medium. Furthermore, roles or the promotional effects of Fe and melamine are intensively investigated, and some interesting results have been obtained.

## 2. Experimental

### 2.1. Catalysts preparation

Preparation of hybrid precursor Fe/*o*PD–Mela: In a typical approach, 12.0 g melamine, 3.0 g *o*-phenylenediamine (*o*PD) and 1.45 g $FeCl_3{\cdot}6H_2O$ (the ratio of the Fe is 2 wt% of the melamine and *o*-phenylenediamine) were first dispersed in 500 ml 0.75 M HCl solution and the mixture was fierce stirred in an ice bath and then 6.0 oxidant ammonium peroxydisulfate (APS) was dispersed in 100 ml 0.75 M HCl solution and adds into the mixture. After constant stirring for 18 h below 10 °C for the completely polymerization of *o*-phenylenediamine, the mixture was vacuum drying to remove the solvent. Followed the hybrid precursor was pyrolyzed at 900 °C in an argon atmosphere for 1.0 h. Then the sample was leached in 1.0 M $H_2SO_4$ at 80 °C for 6 h, followed by thoroughly washing with de-ionized water. The resulting suspension 0.2 g was firstly ultrasonically dispersed in 15 ml ethanol for about 2–3 h and then the resulting suspension was spread onto an evaporating dish and dried at room temperature (RT). Finally, the catalyst was obtained by pyrolyzing the sample, which has been ultrasound, in argon atmosphere for 1.0 h; we denote the catalyst as Fe/*o*PD–Mela.

For comparison, we prepared a series of doped catalysts with almost same procedures, such as Fe/*o*PD and Fe/Mela prepared without the addition of melamine or *o*PD at 900 °C, and C–Mela prepared by pyrolyzing from pure melamine at 600 °C, respectively.

Unless otherwise specified, for all the catalyst samples, the ratio of *o*PD to melamine is 1:4 by weight, and the Fe content in the hybrid precursor is ca. 2 wt%.

The ORR performances of the catalysts were evaluated on an electrochemical workstation (Ivium, Netherlands) at RT (25 ± 1 °C), using a three-electrode electrochemical cell. The work electrode was prepared with the following procedures: 5 mg catalysts were dispersed ultrasonically in 1 ml (or 2 ml) Nafion/ethanol (0.25 wt% Nafion) for 30 min, then 20 μl (or 5 μl) catalyst dispersion was pipetted and spread on the glassy carbon electrode (5 mm inner diameter), the doped carbon catalyst loadings: 0.51 mg $cm^{-2}$ (or JM Hispec 4100, Pt/C catalyst, the loadings are 25 μg Pt $cm^{-2}$), followed by drying under an infrared bulb. A graphite rod and Ag/AgCl (3 M KCl) were used as the counter and reference electrodes, respectively, the potential of the Ag/AgCl (3 M KCl) was calibrated with a RHE reference electrode (in 0.1 M KOH, $E$ (RHE) = $E$ (Ag/AgCl) + 0.982 V; in 0.1 M $HClO_4$, $E$ (RHE) = $E$ (Ag/AgCl) + 0.288 V). ORR steady-state polarization measurements were conducted in $O_2$-saturated 0.1 M KOH electrolyte with scanning rates of 10 mV $s^{-1}$.

The steady-state chronoamperometric response was tested at the polarizing potential of 0.68 V in the $O_2$-saturated electrolyte. 2.0 ml mixed solutions (0.1 M KOH + 3 M methanol) into the electrolyte (ca. 60 ml) after about 220 s (the test is paused 2 min to mix the solution uniform) to examine the methanol crossover. And durability testing of the Fe/*o*PD–Mela electrode and Pt/C electrocatalyst was conducted by the chronoamperometric technique at 0.68 V in an $O_2$-saturated aqueous solution of 0.1 M KOH for up to 30,000 s.

The sing $H_2$/air PEM fuel cell test was conducted in a test cell with an Arbin fuel cell testing system (Arbin, USA). The doped carbon catalyst Fe/*o*PD–Mela or Fe/*o*PD were used as the cathode, the MEA with an active area of 5.0 $cm^2$ were fabricated using the catalyst-sprayed membrane method reported previously by our group [45]. In a typical approach, the slurry of catalyst slurry was sprayed on one side of a Nafion 212 membrane (DuPont, USA) to form the cathode catalyst layer and the commercial Hispec 4100 Pt/C catalyst was used as an anode catalyst. The doped carbon catalyst (or Pt) loadings in the cathode were 3 mg $cm^{-2}$ (or 0.2 mg Pt $cm^{-2}$) and Pt loadings in the anodes were 0.1 mg $cm^{-2}$, respectively. The dry Nafion (DuPont, USA) content in both anode and cathode catalyst layer (CL) was 25 wt%. Finally, two pieces of gas diffusion layers (GDLs) were pressed on both sides to form a MEA with doped carbon catalyst as cathode and Pt/C as anode. The GDLs for anode and cathode were prepared with the procedures we previously reported [45]. $H_2$ and air were fed as the fuel and oxidant with fully humidified at 30 psi back pressure, and the cell temperature is controlled at 80 °C.

### 2.2. Characterization

XRD was conducted on a TD-3500 powder diffractometer (Tongda, China) operated at 40 kV and 30 mA, using Cu-*K*α radiation sources. Thermogravimetry (TG) analyses were performed on a Q600 SDT (TA Inc. USA) analyzer in the flowing of pure nitrogen (100 ml $min^{-1}$), with heating velocity of 10 °C/min from room temperature to 900 °C. Specific surface areas were measured by Brunauer–Emmett–Teller (BET) nitrogen adsorption-desorption on a TristarII 3020 (Micromeritics, USA) gas adsorption analyzer. TEM images were recorded on a JEM-2100HR microscope (JEOL, Japan) operated at 200 kV. SEM was conducted with a Nova Nano Scanning Electron Microscope 430 (Quantum Design, USA) operated at 10 kV. X-ray photoelectron spectroscopy (XPS) was performed on an Axis Ultra DLD X-ray photoelectron spectrometer (Kratos, England) employing a monochromated Al-*K*a X-ray source ($h\nu$ = 1486.6 eV). The Mössbauer spectra were recorded at room temperature with a Topologic 500A spectrometer. The $^{57}$Co(Rh) source is moving in a constant acceleration model.

## 3. Results and discussion

### 3.1. Morphology and structure

Fig. 1a compares the XRD patterns of several samples pyrolyzed from various precursors. The C–Mela sample was prepared from pure melamine; the Fe/*o*PD was prepared by using almost the same procedures as for Fe/*o*PD–Mela but without the addition of melamine in the precursor. C–Mela shows a strong, narrow diffraction peak of 27.6° at 2$\theta$, which may be correlated to the (0 0 2) peak of carbon, implying that the doped carbon pyrolyzed from melamine has good orderliness, with shorter interlayer spacing

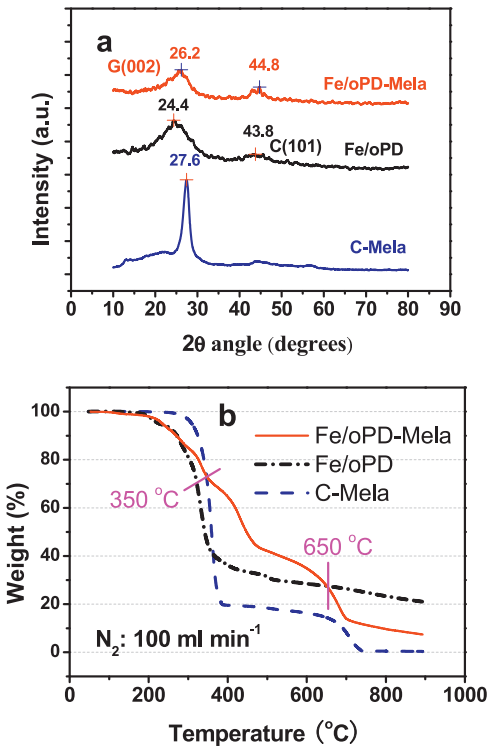


**Fig. 1.** (a) XRD patterns of Fe/*o*PD–Mela, Fe/*o*PD, and C–Mela, pyrolyzed and graphitized at 900 °C; (b) TG curves of the precursors of C–Mela, Fe/*o*PD and Fe/*o*PD–Mela catalysts, in the flowing of pure nitrogen with a temperature rating of 10 °C min$^{-1}$.

(0.323 nm) compared to the other two samples. The Fe/*o*PD shows a weak, widened peak at 24.4° (interlayer spacing: 0.355 nm), possibly revealing a disordered structure of this doped carbon catalyst. It is interesting that in the case of Fe/*o*PD–Mela, prepared from a precursor by mixing melamine with iron salts and *o*PD, the shape of the (0 0 2) peak resembles that of Fe/*o*PD but shifts to 26.2° at 2θ – between the values for C–Mela and Fe/*o*PD – indicating the significant structural effect of adding melamine. The interlayer spacing (0.340 nm) located between that of melamine derived carbon (0.323 nm) and Fe/*o*PD (0.355), it is very close to that of single-layer graphene (0.335 nm) [46]. It may indicate that the structure changed from that of Fe/*o*PD and formed a nitrogen-doped graphene structure after the doping of melamine.

Fig. 1b shows TG spectra of the precursors of C–Mela, Fe/*o*PD and Fe/*o*PD–Mela in pure nitrogen. It is interesting that the TG spectrum of Fe/*o*PD–Mela is not a simple sum of both of Mela and Fe/*o*PD. We find that weight loss of the Fe/*o*PD–Mela precursor is less than those of C–Mela and Fe/*o*PD precursors from 350 °C to 650 °C, and the precursor of Fe/*o*PD–Mela obviously experienced a much complex pyrolyzing process than the precursors of Mela and Fe/*o*PD, which may be related to the formation of graphene structure of the catalysts.

The $N_2$-sorption isotherm (Fig. 2a) of the three samples yields a type-I curve with a wide platform in its middle. Their adsorption amounts follow the order of Fe/*o*PD–Mela > Fe/*o*PD > C–Mela, implying the Fe/*o*PD–Mela has more pore volume than Fe/*o*PD and C–Mela. Also, for sample Fe/*o*PD–Mela, there is a sharp upward turning at the tail, and a small hysteresis loop, indicating the catalyst may have narrow pore size distribution. As shown Fig. 2b, the BET surface areas calculated from the isotherms are 10, 91 and 384 $m^2 g^{-1}$ for C–Mela, Fe/*o*PD and Fe/*o*PD–Mela, respectively. It clearly revealed that the addition of melamine could enhance the BET surface area of the catalyst significantly. It can be expected that the high surface area of the catalyst caused by the addition of Fe and melamine will contribute to the performance enhancement.

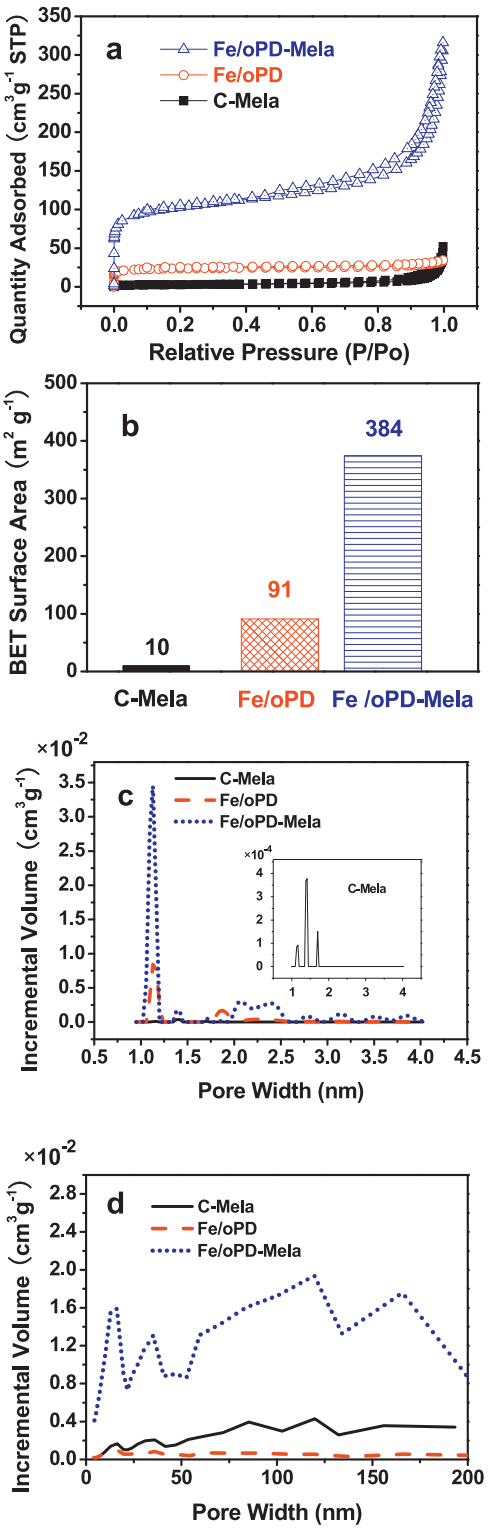


**Fig. 2.** (a) $N_2$ sorption/desorption isotherms, (b) the BET surface area, (c) Density functional theory adsorption pore distribution (0.9 nm to 4 nm) and (d) Barrett–Joyner–Halenda adsorption pore distribution (4 nm to 200 nm) of C–Mela, Fe/*o*PD, Fe/*o*PD–Mela.

Fig. 2c and d shows pore distribution of C–Mela, Fe/*o*PD and Fe/*o*PD–Mela. It is clearly that the micropores, mesopores and macropores are co-existed in the Fe/*o*PD–Mela catalyst, but the

**Table 1**
The XPS elemental content analysis of nitrogen, carbon, oxygen and sulfur and iron element for C–Mela, Fe/*o*PD and Fe/*o*PD–Mela.

| Sample | N (at%) | C (at%) | O (at%) | S (at%) | Fe (at%) |
|---|---|---|---|---|---|
| C–Mela | 51.48 | 46.34 | 2.18 | 0.0 | 0.0 |
| Fe/*o*PD | 5.51 | 78.50 | 12.93 | 1.83 | 1.22 |
| Fe/*o*PD–Mela | 6.83 | 84.53 | 6.96 | 0.57 | 1.12 |

main pore size is focused on 1.13 nm. After the doping of melamine, the pore distribution peak at 1.13 nm of Fe/*o*PD–Mela catalyst greatly enhanced compared with that of Fe/*o*PD, confirming the effects of melamine on the pore structure of the Fe/*o*PD–Mela catalyst. The significant enhancements in surface area and pore volume for the Fe/*o*PD–Mela may result from the formation of the graphene-like structure of the catalyst after the doping of melamine.

Furthermore, we believe that the high surface area and rich porosity caused by the addition of melamine may be two important factors in the enhancement of the catalyst's ORR activity.

Another significant effect of melamine on the catalyst is the relative content of pyridinic N and graphitic N, as shown in Fig. 3. By deconvoluting the XPS spectra of N1s of Fe/*o*PD (Fig. 3a) and Fe/*o*PD–Mela (Fig. 3b), we can assign the four peaks at 398.3 ± 0.2, 399.4 ± 0.2, 400.5 ± 0.6, and 401.7 ± 0.2 eV to pyridinic N [47], N—Fe compounds [48,49], graphitic N [47], and oxidized nitrogen species [50], respectively. The XPS spectra of N1s of C–Mela (Fig. 3c) can be deconvoluted into two components at around 397.8 and 399.3 eV, according to the literature, these two peaks could be attributed to C—NH (and/or C—$NH_2$) and C=N—C bonds [51,52]. Although the C–Mela contains large amounts of nitrogen (51.48 wt%, see Table 1), but its performance is very poor. It can be explained by following two reasons: (i) the C—N structure in the C–Mela maybe not the active site of ORR activity, (ii) the poor conductivity of C–Mela. Interestingly, with the addition of melamine to the precursor, the relative content (at%) of inactive oxidized N species decreases sharply from 41.2 at% of Fe/*o*PD to 17.8% of Fe/*o*PD–Mela, and the active pyridinic N and graphitic N [15,27,53,54] increase from 11.8 at% and 27.5 at% to 27.5 at% and 35.1 at%, respectively (Fig. 3d). Additionally, the total nitrogen content is also increased by the addition of melamine to the precursor, total pyridinic N and graphitic N content of Fe/*o*PD–Mela are 4.28 wt% which is 1.97 times to that of the Fe/*o*PD (2.17 wt%), demonstrating that melamine doped into the precursor can enhance the content of doped nitrogen and the chemical status of the doped nitrogen in the final product. We can expect that these changes will result in significant catalyst performance enhancement.

Fig. 4 shows SEM and TEM images of Fe/*o*PD–Mela and Fe/*o*PD. As is evident in Fig. 4a, doped carbon material exhibits crinkled nanostructures, while Fig. 4c reveals a graphene-like structure, in which very thin, transparent nanosheets are clearly observable. In Fig. 4d we can clearly see graphite lines and wrinkles which further confirm Fe/*o*PD–Mela has a graphene-like structure. However, we cannot see any graphene structure from the SEM images of Fe/*o*PD (Fig. 4b), indicating that the melamine plays a crucial role in the formation of graphene-like structure of the Fe/*o*PD–Mela catalyst. This phenomenon also has been investigated by some researchers, Li et al. [19] reported that some blocks were formed when the *o*PD was pyrolyzed with Fe as catalyst; and Zhang et al. [35] also reported the important role of melamine in the formation of high performance doped carbon composite catalyst.

It should be pointed out that no nanoparticles of iron or iron oxide can be observed in the SEM or TEM images of the Fe/*o*PD–Mela sample, which is quite consistent with the XRD results, however, the results of XPS revealed its existence (Table 1). We believe most iron may be removed in the process of acid leaching, and only a few Fe atoms are remained in the final catalyst samples. As for the role of Fe, we suggested that it plays as a catalyst in the pyrolysis process, and the residual iron may play as a component for the active centre.

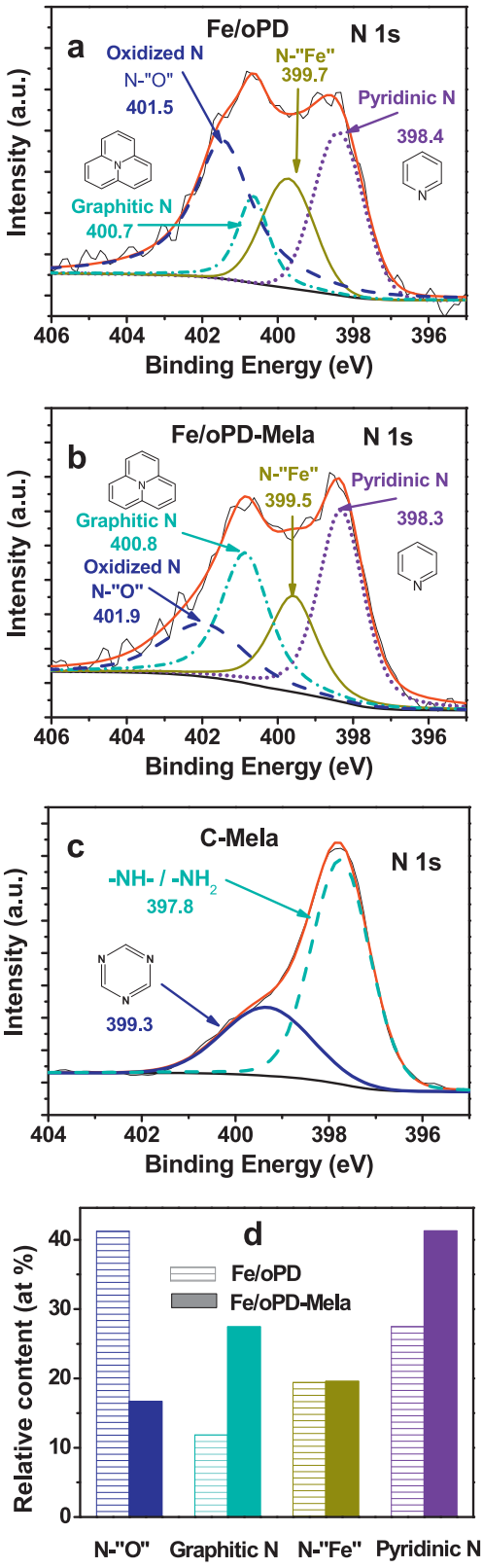


**Fig. 3.** High-resolution XPS spectra of N1s for: (a) Fe/*o*PD and (b) Fe/*o*PD–Mela; (c) C–Mela. (d) Column diagram of the relative content (at%) of various types of nitrogen of: Fe/*o*PD (spare line) and Fe/*o*PD–Mela (solid).

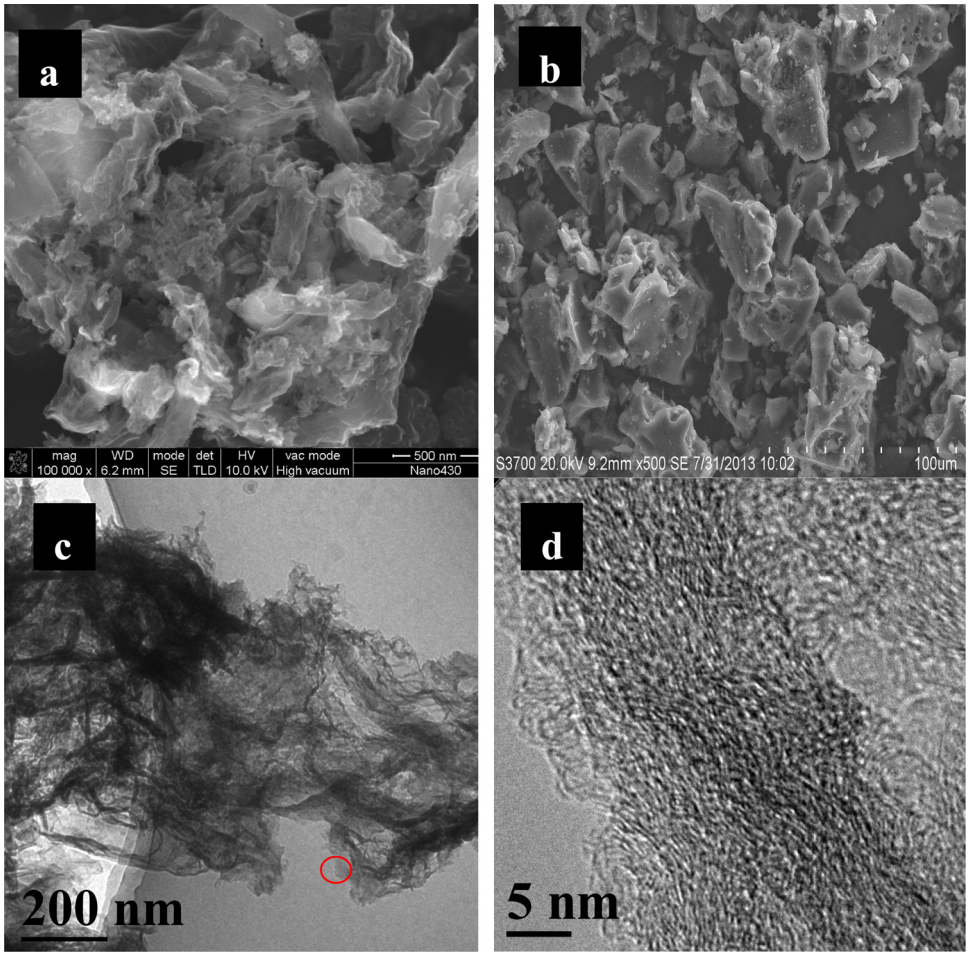


**Fig. 4.** SEM images of: (a) Fe/*o*PD–Mela, (b) Fe/*o*PD; and TEM images of Fe/*o*PD–Mela (c and d) catalyst.

To further understand the role of residual iron in the catalyst, $^{57}$Fe Mössbauer spectroscopy measurement has been carried out. For Fe/*o*PD sample without melamine addition, its spectrum can be deconvolved into three doublet peaks and one sextet line (see Fig. 5a and Table 2). Doublet 1 can be assigned to $FeS_2$ and/or $FeO_x$ species [55,56] and which contribute ca. 69.4% in Fe/*o*PD, doublet 2, and doublet 3 may be associated with Fe:S clusters [57] and distorted Fe-$N_4$ [36,58], and they contribute ca. 10.9% and 7.1%, respectively. And the sextet can be assigned to $Fe_5C_2$ [36,59] and the contribution of it is 12.6%.

However, for Fe/*o*PD–Mela catalyst, the situation is quite different, its spectrum can be deconvolved into two doublet and one sextet line. Doublet 1 and doublet 2 can be assigned to in-plane $FeN_4$ structures [35,58] and $CFeN_2$ and/or $[FeN_4]^{2-}$ [60], and which contribute ca. 44.1% and 35.0% in Fe/*o*PD–Mela, respectively. And the sextet can be associated with $Fe_3O_4$ [59,61] and the contribution of it is 20.9%.

For Fe/*o*PD–Mela catalyst, the content of Fe existed as Fe—N and C—Fe—N species is up to 79.1%, but for Fe/*o*PD sample, it is only 7.1%, most of Fe existed as Fe—S and Fe—O species. Fe—N and C—Fe—N species are generally recognized as active related species or component of the active centre of doped carbon catalyst [35,60]. The high content of Fe—N and C—Fe—N species in Fe/*o*PD–Mela catalyst reveals that melamine plays as an excellent nitrified agent in the pyrolysis process, and it may be one of the most important reasons for the high enhancement of melamine. Actually, this result is consistent with the XPS results and in which we found that Fe/*o*PD–Mela has higher pyridinic N content than that of the Fe/*o*PD. Zhang et al. [36] found that there was an approximately linear relationship between the ORR activity and the percentages of Fe—$N_4$ and $CFeN_2$.

**Table 2**
Mössbauer parameters and their assignments for various samples at room temperature.

| Samples | | $\delta_{iso}$ (mm s$^{-1}$) | $E_Q$ (mm s$^{-1}$) | $H_0$ (T) | Real area $A$ (%) | Assignment | Refs. |
|---|---|---|---|---|---|---|---|
| Fe/*o*PD | Doublet 1 | 0.31 | 1.5 | | 69.4 | $FeS_2$ and/or $FeO_x$ | [55,56] |
| | Doublet 2 | 0.85 | 1.92 | | 10.9 | Fe:S clusters | [57] |
| | Doublet 3 | 0.40 | 3.71 | | 7.1 | Fe—$N_4$ (distorted) | [36,58] |
| | Sextet | 0.25 | −0.05 | 48.97 | 12.6 | $Fe_5C_2$ | [36,59] |
| Fe/*o*PD–Mela | Doublet 1 | 0.36 | 1.02 | | 44.1 | Fe—$N_4$ (in-plane) | [35,58] |
| | Doublet 2 | 0.52 | 2.53 | | 35.0 | $CFeN_2$ and/or $[FeN_4]^{2-}$ | [60] |
| | Sextet | 0.55 | −0.04 | 25.25 | 20.9 | $Fe_3O_4$ | [59,61] |

### 3.2. Activities and stabilities for ORR

As shown in Fig. 6a and b, although C–Mela may have high doped-nitrogen content, it exhibits very poor ORR activity; Fe/*o*PD and Fe/Mela also demonstrates very low activity. However, once the precursor contains melamine, *o*PD, and iron, Fe/*o*PD–Mela displays unexpectedly high ORR activity. Indeed, its performance surpasses that of Pt/C catalyst in an alkaline medium (Fig. 6a), with a half-wave potential about 50 mV higher than that of the latter. The current density at 0.9 V for Fe/*o*PD–Mela is about 2.4 times to that of the above described Pt/C catalyst. As shown in Fig. 6b, the Fe/*o*PD–Mela catalyst also exhibited excellent ORR activity in an acid medium; its half-wave potential is only 62 mV less than that of the Pt/C catalyst.

Fig. 6c shows the effects of pyrolysis temperature on the catalyst's performance, the optimal temperature apparently being 900 °C. Fig. 6d shows that the ratio of *o*PD to melamine has a significant effect on the ORR activity. Activity increases as more melamine is added to the precursor, with activity peaking at an *o*PD/melamine ratio of 1:4; when the ratio reaches 1:8, the activity decreases significantly. These results further confirm that melamine plays a key role in the formation of active sites for these doped carbon catalysts.

Fig. 6e clearly shows that 2 wt% of iron added in the precursor is optimal for our Fe/*o*PD–Mela catalyst, as more iron does not yield further performance enhancement. However, if no iron is present, the catalyst exhibits poor activity, whereas once 1 wt% of iron is added, the activity greatly improves. Iron clearly plays an important role in the high performance of Fe/*o*PD–Mela.

Why ORR activity of Fe/*o*PD–Mela is much higher than those of C–Mela, Fe/*o*PD and Fe/Mela? We speculated possible reasons as follows: (i) high doped N amount due to the addition of melamine; (ii) the graphene structure and high surface area due to the addition of melamine and Fe; (iii) most of remained Fe was existed as active Fe—N and C—Fe—N species.

Fig. 6f shows the single fuel cell performances of a MEA with Fe/*o*PD–Mela as the cathode, and a MEA with JM Pt/C as cathode. Compared with the MEA with JM Pt/C as cathode, the current density of the Fe/*o*PD–Mela is only about 41% of that of the Pt/C catalyst at 0.8 V (Fig. 6b); and the maximum power density of Fe/*o*PD–Mela is 0.27 W $cm^{-2}$, which is only 44% of that of the Pt/C catalyst (Fig. 6f), revealing that the performances of Fe/*o*PD–Mela in both cyclic voltammetry (CV) and PEM fuel cell testing, are still much lower than that of commercial Pt/C catalysts in acidic medium, especially in an acidic PEM fuel cell [28,34,62]. In other words, there is a big gap need to be overcome for the practical application of doped carbon catalyst. However, it should be pointed out that the PEM fuel cell performance of our Fe/*o*PD–Mela catalyst is among the best ones produced so far [12,34,63,64]. Additionally, we found that the single $H_2$-air PEM fuel cell performance of Fe/*o*PD–Mela was much higher than that of the Fe/*o*PD which open cell voltage was 0.67 V and the maximum power density was 1.42 mW $cm^{-2}$. These are shown that the melamine doped to Fe/*o*PD can significantly improve the single $H_2$-air PEM fuel cell performance.

That Fe/*o*PD–Mela is insensitive to methanol is helpful for the cathode catalyst of methanol fuel cells, as the catalyst will tolerate methanol crossover from the anode side. As shown in Fig. 7a, after the addition of 2.0 ml mixed solutions (0.1 M KOH + 3 M methanol) into the electrolyte (ca. 60 ml), the ORR current density for the Fe/*o*PD–Mela catalyst remains almost unchanged; in contrast, the ORR current density for the Pt/C catalyst suffers a sharp decrease of 50%. This demonstrates that Fe/*o*PD–Mela has good methanol tolerance, making it a fine candidate for the cathode of direct methanol fuel cells.

Fe/*o*PD–Mela was also evaluated using a chronoamperometric durability test of the ORR in $O_2$-saturated 0.1 M KOH solution (Fig. 7b). The current signal decayed about 14% of Pt/C after continuous oxygen reduction (for ca. 30,000 s) at 0.68 V, whilst only a slight loss (2%) of current density was recorded on Fe/*o*PD–Mela, indicating the high stability of our catalyst towards the ORR.

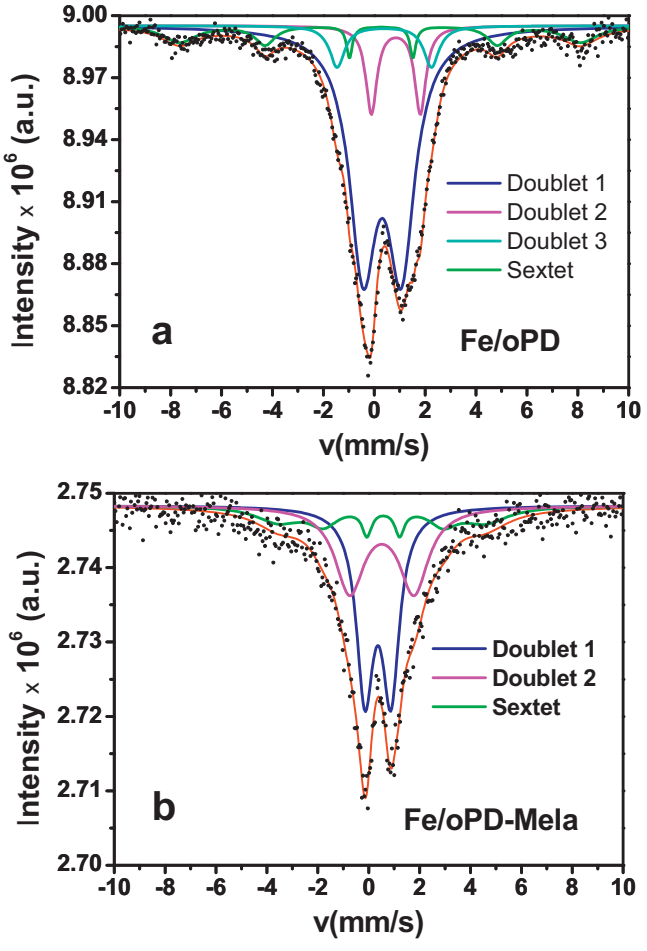


**Fig. 5.** Mössbauer spectrums of (a) Fe/*o*PD and (b) Fe/*o*PD–Mela measured at room temperature.

### 3.3. Reaction mechanism analysis

The kinetics of ORR on Fe/*o*PD (Fig. 8a) and Fe/*o*PD–Mela (Fig. 8b) were investigated by changing the rotation speed of the electrode from 900 to 3600 rpm. According to the Koutecky–Levich equation as below,

$$\frac{1}{J} = \frac{1}{J_{kin}} + \frac{1}{J_{diff}} = \frac{1}{J_{kin}} + \frac{1}{B \times \sqrt{\omega}} \quad (1)$$

In Eq. (1), the current density ($J$) consists of a kinetic part ($J_{kin}$) and a diffusion part ($J_{diff}$), $\omega$ is the angular velocity of the disk ($\omega = 2\pi N$, $N$ is the linear rotation rate). Plot of $J^{-1}$ versus $\omega^{-1/2}$ at each potential, we can obtain $J^{-1}$-$\omega^{-1/2}$ lines. B is a constant, as shown in Eq. (2)

$$B = 0.62 \times n \times F \times D^{2/3} \times \nu^{-1/6} \times C \quad (2)$$

where $n$ is the number of electrons transferred during the ORR, $F$ is the Faraday constant ($F = 96485$ C $mol^{-1}$), $D$ is the diffusion coefficient of $O_2$ in the 0.1 M KOH electrolyte ($D = 1.9 \times 10^{-5}$ $cm^2$ $s^{-1}$), C is the bulk concentration of $O_2$ ($C = 1.2 \times 10^{-3}$ mol $l^{-1}$), $\nu$ is the kinetic viscosity of the electrolyte ($\nu = 1.0 \times 10^{-2}$ $cm^2$ $s^{-1}$) [65].

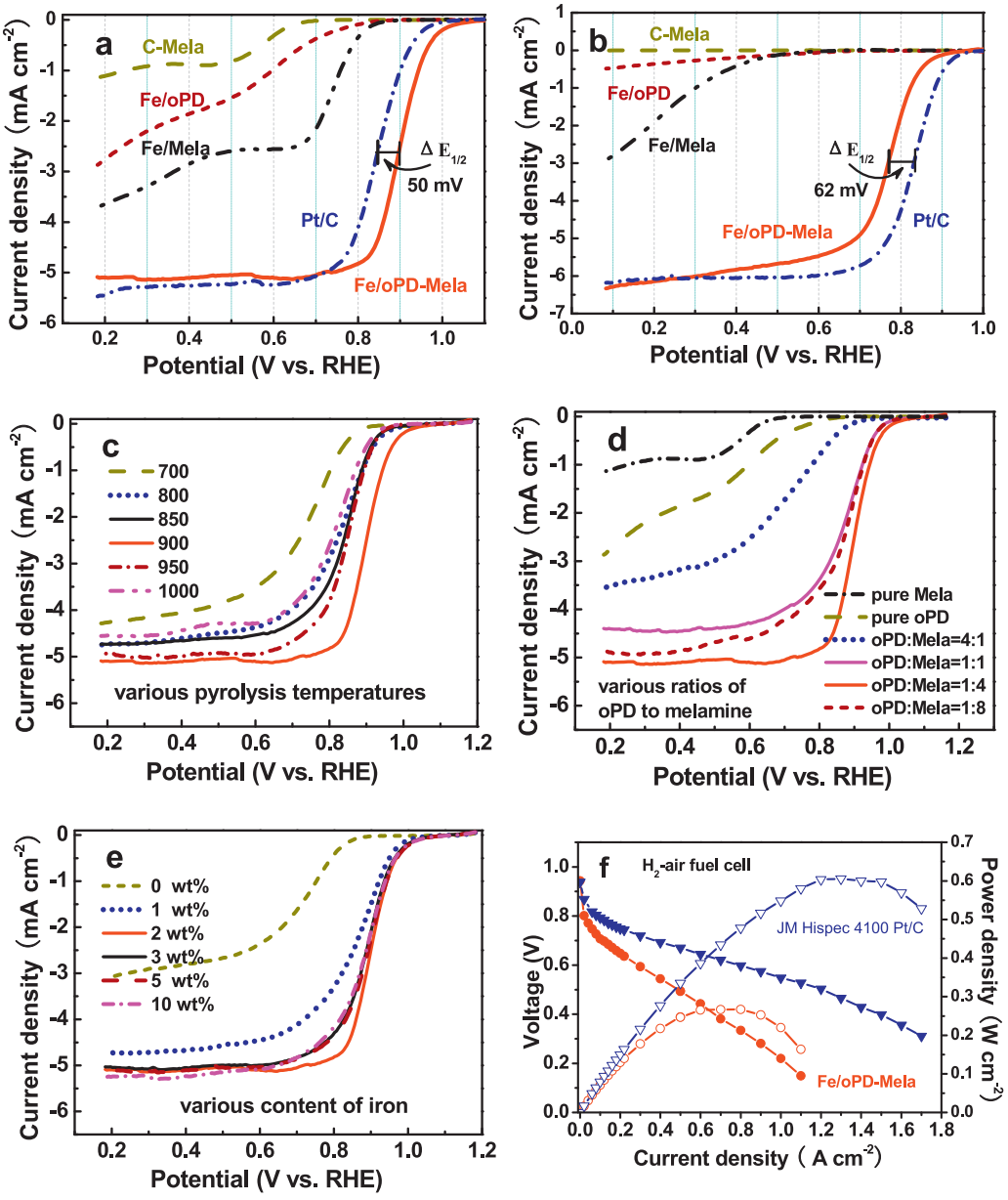


**Fig. 6.** Linear sweep voltammetry curves of C–Mela, Fe/*o*PD, Fe/Mela, Pt/C and Fe/*o*PD–Mela (a) in $O_2$-saturated 0.1 M KOH (b) in $O_2$-saturated 0.1 M $HClO_4$; (c) Fe/*o*PD–Mela with various pyrolysis temperatures, (d) Fe/*o*PD–Mela with various ratios of *o*PD to melamine, (e) Fe/*o*PD–Mela with various content of iron, in $O_2$-saturated 0.1 M KOH with a scanning rate of 10 mV $s^{-1}$ and a rotation speed of 1600 rpm for the electrode. (f) Polarization plots of a single $H_2$-air PEMFC with Fe/*o*PD–Mela as the cathode (loading: 3 mg $cm^{-2}$) and with JM Pt/C as cathode (Pt loading: 0.2 mg $cm^{-2}$), the Pt loading at anode: 0.1 mg $cm^{-2}$.

According to Eqs. (1) and (2), we calculated the electron transfer number $n$ from the slope of each line, the average value of is 2.1 and 3.7 for Fe/*o*PD and Fe/*o*PD–Mela catalysts, respectively. It seems that the addition of melamine to the precursor changes the ORR reaction mechanism; this is a very significant and interesting finding with respect to our catalyst, and requires a further, intensive investigation.

Fig. 8c shows the mass transport-corrected Tafel plots for Fe/*o*PD and Fe/*o*PD–Mela in 0.1 M KOH at 1600 rpm. Tafel plots are obtained after the measured currents are corrected and calculated from Eq. (3) [66].

$$J_{kin} = J \times \frac{J_{diff}}{(J_{diff} - J)} \quad (3)$$

The Tafel slope is 85 and 78 mV $dec^{-1}$ for Fe/*o*PD and Fe/*o*PD–Mela catalysts at 1600 rpm, respectively. Both these values are different from the Tafel slope for the ORR on Pt in 0.1 M KOH (ca. 60 mV $dec^{-1}$) [67]. These suggest that ORR mechanism of Fe/*o*PD and Fe/*o*PD–Mela are quite different from the Pt. The difference in Tafel slope values for Fe/*o*PD and Fe/*o*PD–Mela also indicate a different nature of the active ORR site in them. The Fe/*o*PD–Mela has a lower Tafel slope than that of the Fe/*o*PD. And this show that the Fe/*o*PD–Mela has lower overpotential than that of the Fe/*o*PD, at the same kinetic current density. Fig. 8c also shows the Fe/*o*PD–Mela could yield the larger value of the exchange current density than the Fe/*o*PD and led in better ORR activity.

Based on the above discussion, a schematic diagram describing the catalyst synthesis is suggested as Scheme 1. If no melamine was added, the Fe/*o*PD catalyst was prepared by following procedures, firstly, *o*PD was completely polymerization in 0.75 M HCl solution, containing transition metal iron as catalyst, and APS as an oxidant, to form a Fe mixed polymer poly (*o*-phenylenediamine) (p-*o*PD)

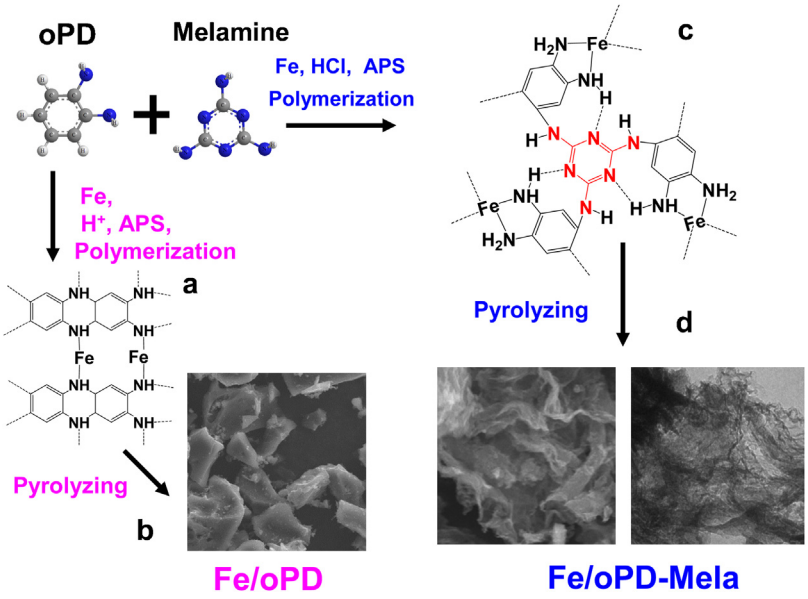


**Scheme 1.** Schematic diagram of the synthesis of Fe/*o*PD and Fe/*o*PD–Mela catalysts.

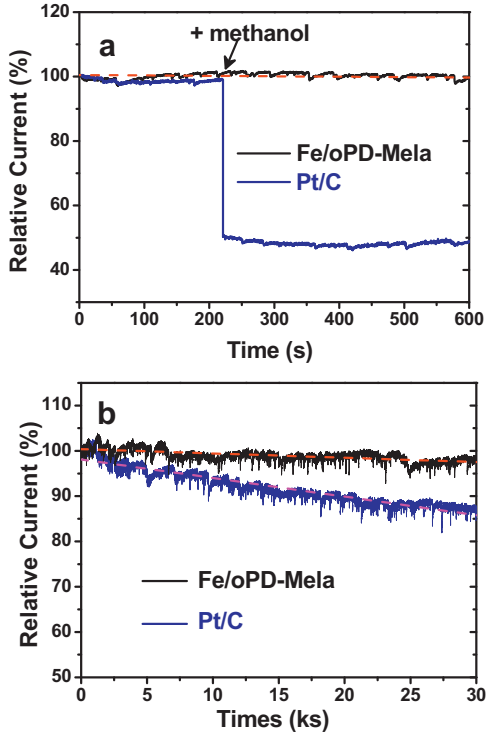


**Fig. 7.** Chronoamperometric response for the ORR at Fe/*o*PD–Mela and Pt/C electrodes: (a) with the addition of methanol to the electrolyte after about 220 s at 0.68 V; (b) durability evaluation of Fe/*o*PD–Mela and Pt/C electrodes for 30,000 s at 0.68 V and a rotation rate of 900 rpm, in $O_2$-saturated 0.1 M KOH.

(a), then the Fe/*o*PD catalyst was prepared by pyrolyzing Fe mixed p-*o*PD polymer material at 900 °C, this catalyst shows bulk appearance and with low surface area (b). This results is consistent with that reported by Zhu et al. [68], their prepared Fe doped p-*o*PD carbon catalyst also presents agglomerate structure and low BET surface area of ca. 72 $m^2\ g^{-1}$.

However, when excessive amounts of melamine add into the precursors, a Fe mixed co-polymers of melamine and *o*PD was obtained firstly (c), followed by a pyrolysis process at 900 °C,

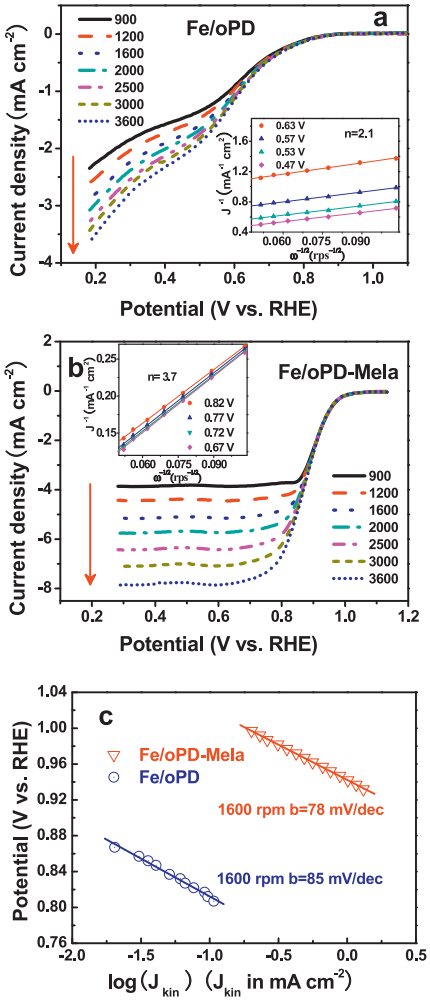


**Fig. 8.** ORR polarization plots of (a) Fe/*o*PD and (b) Fe/*o*PD–Mela catalyst in $O_2$-saturated 0.1 M KOH electrolytes at different rotation rates and the Koutecky–Levich plots (inset); (c) Tafel plots for oxygen reduction on Fe/*o*PD and Fe/*o*PD–Mela catalyst.

a fluffy, irregular graphene-like materials Fe/*o*PD–Mela can be obtained (d).

Melamine may play two roles for the formation of the high performance catalyst: (i) as a nitrogen source which can increase the nitrogen content and adjusting the valence bond structure of nitrogen in the final product (Fig. 3, Table 1), which make the active pyridinic N and graphitic N content of Fe/*o*PD–Mela increased to 1.97 times to that of the Fe/*o*PD. Also, melamine may facilitate the incorporation of N atom into the matrix of graphitized carbon; (ii) resulting in the formation of graphene like structure of the catalyst, which increases the BET surface area and porosity of the catalyst. As shown in Fig. 2, the BET surface area of Fe/*o*PD–Mela is about 4.2 times to that of the Fe/*o*PD.

## 4. Conclusions

In conclusion, we have prepared a doped carbon catalyst Fe/*o*PD–Mela by pyrolyzing a hybrid precursor of poly *o*-phenylenediamine (*o*PD), melamine and iron in an Ar atmosphere. This catalyst exhibits ultra high ORR activity, good durability and tolerance towards methanol, its activity surpasses that of commercial Pt/C in alkaline medium, and comparable with Pt/C catalyst in acid medium. It was revealed that the addition of melamine plays an important role for the high performance of the catalyst, increasing the content of active nitrogen species, improving the formation of graphene structure, and facilitating the incorporation of N atom into the matrix of graphitized carbon. Furthermore, the added Fe also plays an important role for the high ORR activity of the catalyst, it acted as catalyst in the pyrolysis process for the formation of graphene structure and the active centres; whilst, it may function as a component for the formation of active species or active centre, e.g. forming Fe–$N_4$ and $CFeN_2$ structures species.

## Acknowledgements

The authors would like to acknowledge the financially supported of the National Science Foundation of China (NSFC Project Nos. 20876062, 21076089, 21276098, 11132004), Guangdong Natural Science Foundation (Project No S2012020011061), Doctoral Fund of Ministry of Education of China (20110172110012), and Doctoral Fund of Department of Education of Guangdong.

## References

[1] M.K. Debe, Nature 486 (2012) 43–51.
[2] S. Sun, G. Zhang, N. Gauquelin, N. Chen, J. Zhou, S. Yang, W. Chen, X. Meng, D. Geng, M.N. Banis, R. Li, S. Ye, S. Knights, G.A. Botton, T.K. Sham, X. Sun, Sci. Rep. 3 (2013) 1775.
[3] M. Escudero-Escribano, A. Verdaguer-Casadevall, P. Malacrida, U. Gronbjerg, B.P. Knudsen, A.K. Jepsen, J. Rossmeisl, I.E.L. Stephens, I. Chorkendorff, J. Am. Chem. Soc. 134 (2012) 16476–16479.
[4] S. Liao, K.A. Holmes, H. Tsaprailis, V.I. Birss, J. Am. Chem. Soc. 128 (2006) 3504–3505.
[5] O.H. Kim, Y.H. Cho, S.H. Kang, H.Y. Park, M. Kim, J.W. Lim, D.Y. Chung, M.J. Lee, H. Choe, Y.E. Sung, Nat. Commun. 4 (2013) 2473.
[6] N. Jung, S.M. Kim, D.H. Kang, D.Y. Chung, Y.S. Kang, Y.H. Chung, Y.W. Choi, C. Pang, K.Y. Suh, Y.E. Sung, Chem. Mater. 25 (2013) 1526–1532.
[7] S.J. Hwang, S.J. Yoo, J. Shin, Y.H. Cho, J.H. Jang, E. Cho, Y.E. Sung, S.W. Nam, T.H. Lim, S.C. Lee, S.K. Kim, Sci. Rep. 3 (2013) 1309.
[8] H.Y. Park, T.Y. Jeon, J.H. Jang, S.J. Yoo, K.H. Choi, N. Jung, Y.H. Chung, M. Ahn, Y.H. Cho, K.S. Lee, Y.E. Sung, Appl. Catal., B: Environ. 129 (2013) 375–381.
[9] Z. Yao, H. Nie, Z. Yang, X. Zhou, Z. Liu, S. Huang, Chem. Commun. 48 (2012) 1027–1029.
[10] S. Li, Y. Hu, Q. Xu, J. Sun, B. Hou, Y. Zhang, J. Power Sources 213 (2012) 265–269.
[11] P. Pachfule, V.M. Dhavale, S. Kandambeth, S. Kurungot, R. Banerjee, Chem. Eur. J. 19 (2013) 974–980.
[12] Z. Chen, D. Higgins, A. Yu, L. Zhang, J. Zhang, Energy Environ. Sci. 4 (2011) 3167–3192.
[13] Y. Hu, X. Zhao, Y. Huang, Q. Li, N.J. Bjerrum, C. Liu, W. Xing, J. Power Sources 225 (2013) 129–136.
[14] G. Wu, P. Zelenay, Acc. Chem. Res. 46 (2013) 1878–1889.
[15] J. Qiao, L. Xu, L. Ding, L. Zhang, R. Baker, X. Dai, J. Zhang, Appl. Catal., B: Environ. 125 (2012) 197–205.
[16] F. Zheng, G. Mu, Z. Zhang, Y. Shen, M. Zhao, G. Pang, Mater. Lett. 68 (2012) 453–456.
[17] H. Wang, X. Bo, C. Luhana, L. Guo, Electrochem. Commun. 21 (2012) 5–8.
[18] D. Higgins, Z. Chen, Z. Chen, Electrochim. Acta 56 (2011) 1570–1575.
[19] Y. Li, T. Li, M. Yao, S. Liu, J. Mater. Chem. 22 (2012) 10911–10917.
[20] I.Y. Jeon, D. Yu, S.Y. Bae, H.J. Choi, D.W. Chang, L. Dai, J.B. Baek, Chem. Mater. 23 (2011) 3987–3992.
[21] Z. Mo, S. Liao, Y. Zheng, Z. Fu, Carbon 50 (2012) 2620–2627.
[22] Z.H. Sheng, L. Shao, J.J. Chen, W.J. Bao, F.B. Wang, X.H. Xia, ACS Nano 5 (2011) 4350–4358.
[23] A. Zahoor, M. Christy, Y.J. Hwang, Y.R. Lim, P. Kim, K.S. Nahm, Appl. Catal., B: Environ. 147 (2014) 633–641.
[24] H. Meng, F. Jaouen, E. Proietti, M. Lefèvre, J.-P. Dodelet, Electrochem. Commun. 11 (2009) 1986–1989.
[25] E. Proietti, F. Jaouen, M. Lefèvre, N. Larouche, J. Tian, J. Herranz, J.-P. Dodelet, Nat. Commun. 2 (2011) 416.
[26] G. Wu, K.L. More, C.M. Johnston, P. Zelenay, Science 332 (2011) 443–447.
[27] H. Peng, Z. Mo, S. Liao, H. Liang, L. Yang, F. Luo, H. Song, Y. Zhong, B. Zhang, Sci. Rep. 3 (2013) 1765.
[28] D. Deng, L. Yu, X. Chen, G. >S Wang, L. Jin, X. Pan, J. Deng, G. Sun, X. Bao, Angew. Chem. Int. Ed. 52 (2013) 371–375.
[29] K. Gong, F. Du, Z. Xia, M. Durstock, L. Dai, Science 323 (2009) 760–764.
[30] Y. Liang, Y. Li, H. Wang, J. Zhou, J. Wang, T. Regier, H. Dai, Nat. Mater. 10 (2011) 780–786.
[31] H.T. Chung, J.H. Won, P. Zelenay, Nat. Commun. 4 (2013) 1922.
[32] X. Sun, P. Song, Y. Zhang, C. Liu, W. Xu, W. Xing, Sci. Rep. 3 (2013) 2505.
[33] C.H. Choi, M.W. Chung, H.C. Kwon, J.H. Chung, S.I. Woo, Appl. Catal., B: Environ. 144 (2014) 760–766.
[34] J.Y. Cheon, T. Kim, Y. Choi, H.Y. Jeong, M.G. Kim, Y.J. Sa, J. Kim, Z. Lee, T.-H. Yang, K. Kwon, O. Terasaki, G.G. Park, R.R. Adzic, S.H. Joo, Sci. Rep. 3 (2013) 2715.
[35] S. Zhang, H. Zhang, Q. Liu, S. Chen, J. Mater. Chem. A 1 (2013) 3302.
[36] S. Zhang, B. Liu, S. Chen, Phys. Chem. Chem. Phys. 15 (2013) 18482.
[37] Z.S. Wu, S. Yang, Y. Sun, K. Parvez, X. Feng, K. Muellen, J. Am. Chem. Soc. 134 (2012) 9082–9085.
[38] S.Y. Yang, K.H. Chang, Y.L. Huang, Y.F. Lee, H.W. Tien, S.M. Li, Y.H. Lee, C.H. Liu, C.C.M. Ma, C.C. Hu, Electrochem. Commun. 14 (2012) 39–42.
[39] Y. Liang, H. Wang, J. Zhou, Y. Li, J. Wang, T. Regier, H. Dai, J. Am. Chem. Soc. 134 (2012) 3517–3523.
[40] S. Wang, D. Yu, L. Dai, D.W. Chang, J.B. Baek, ACS Nano 5 (2011) 6202–6209.
[41] L. Lai, J.R. Potts, D. Zhan, L. Wang, C.K. Poh, C. Tang, H. Gong, Z. Shen, J. Lin, R.S. Ruoff, Energy Environ. Sci. 5 (2012) 7936–7942.
[42] M. Vikkisk, I. Kruusenberg, U. Joost, E. Shulga, I. Kink, K. Tammeveski, Appl. Catal., B: Environ. 147 (2014) 369–376.
[43] Q. Liu, H. Zhang, H. Zhong, S. Zhang, S. Chen, Electrochim. Acta 81 (2012) 313–320.
[44] Z. Mo, R. Zheng, H. Peng, H. Liang, S. Liao, J. Power Sources 245 (2014) 801–807.
[45] H.N. Su, S.J. Liao, T. Shu, H.L. Gao, J. Power Sources 195 (2010) 756–761.
[46] T.V. Khai, D.S. Kwak, Y.J. Kwon, H.Y. Cho, T.N. Huan, H. Chung, H. Ham, C. Lee, N.V. Dan, N.T. Tung, H.W. Kim, Chem. Eng. J. 232 (2013) 346–355.
[47] X. Li, H. Wang, J.T. Robinson, H. Sanchez, G. Diankov, H. Dai, J. Am. Chem. Soc. 131 (2009) 15939–15944.
[48] J. Ahmed, Y. Yuan, L. Zhou, S. Kim, J. Power Sources 208 (2012) 170–175.
[49] G. Wu, C.M. Johnston, N.H. Mack, K. Artyushkova, M. Ferrandon, M. Nelson, J.S. Lezama-Pacheco, S.D. Conradson, K.L. More, D.J. Myers, P. Zelenay, J. Mater. Chem. 21 (2011) 11392–11405.
[50] D. Choudhury, B. Das, D.D. Sarma, C.N.R. Rao, Chem. Phys. Lett. 497 (2010) 66–69.
[51] I. Louisrose, C. Methivier, J. Vedrine, C. Pradier, Appl. Catal., B: Environ. 62 (2006) 1–11.
[52] A.P. Dementjev, A. de Graaf, M.C.M. van de Sanden, K.I. Maslakov, A.V. Naumkin, A.A. Serov, Diamond Relat. Mater. 9 (2000) 1904–1907.
[53] H. Kim, K. Lee, S.I. Woo, Y. Jung, Phys. Chem. Chem. Phys. 13 (2011) 17505–17510.
[54] R. Liu, D. Wu, X. Feng, K. Müllen, Angew. Chem. Int. Ed. 49 (2010) 2565–2569.
[55] H. Schulenburg, S. Stankov, V. Schünemann, J. Radnik, I. Dorbandt, S. Fiechter, P. Bogdanoff, H. Tributsch, J. Phys. Chem. B 107 (2003) 9034–9041.
[56] J. Xia, J. Jiao, B. Dai, W. Qiu, S. He, W. Qiu, P. Shen, L. Chen, RSC Adv 3 (2013) 6132.
[57] E. Bill, Hyperfine Interact. 205 (2011) 139–147.
[58] U.I. Koslowski, I. Abs-Wurmbach, S. Fiechter, P. Bogdanoff, J. Phys. Chem. C 112 (2008) 15356–15366.
[59] Z. Tao, Y. Yang, C. Zhang, T. Li, M. Ding, H. Xiang, Y. Li, J. Nat. Gas. Chem. 16 (2007) 278–285.
[60] M. Ferrandon, A.J. Kropf, D.J. Myers, K. Artyushkova, U. Kramm, P. Bogdanoff, G. Wu, C.M. Johnston, P. Zelenay, J. Phys. Chem. C 116 (2012) 16001–16013.
[61] K. Shibano, S. Kubuki, K. Akiyama, Z. Homonnay, E. Kuzmann, S. Krehula, M. Ristić, T. Nishida, Hyperfine Interact. (2013) 1–9.
[62] F. Jaouen, E. Proietti, M. Lefèvre, R. Chenitz, J.-P. Dodelet, G. Wu, H.T. Chung, C.M. Johnston, P. Zelenay, Energy Environ. Sci. 4 (2011) 114–130.

[63] D. Zhao, J.L. Shui, C. Chen, X. Chen, B.M. Reprogle, D. Wang, D.J. Liu, Chem. Sci. 3 (2012) 3200.
[64] D.S. Su, G.Q. Sun, Angew. Chem. Int. Ed. 50 (2011) 11570–11572.
[65] Z.W. Liu, F. Peng, H.J. Wang, H. Yu, W.X. Zheng, J. Yang, Angew. Chem. Int. Ed. 50 (2011) 3257–3261.
[66] M. Jahan, Z.L. Liu, K.P. Loh, Adv. Funct. Mater. 23 (2013) 5363–5372.
[67] K. Tammeveski, T. Tenno, J. Claret, C. Ferrater, Electrochim. Acta 42 (1997) 893–897.
[68] H. Zhu, X. Wang, X. Liu, X. Yang, Adv. Mater. 24 (2012) 6524–6529.